ChemPubSoc Europe

DOI: 10.1002/cssc.201701468

CHEMSUSCHEM Full Papers

VIP *Very Important Paper*

Rational Development of Neutral Aqueous Electrolytes for Zinc–Air Batteries

Simon Clark,[a, b] Arnulf Latz,[a, b, c] and Birger Horstmann*[a, b]

Neutral aqueous electrolytes have been shown to extend both the calendar life and cycling stability of secondary zinc–air batteries (ZABs). Despite this promise, there are currently no modeling studies investigating the performance of neutral ZABs. Traditional continuum models are numerically insufficient to simulate the dynamic behavior of these complex systems because of the rapid, orders-of-magnitude concentration shifts that occur. In this work, we present a novel framework for modeling the cell-level performance of pH-buffered aqueous electrolytes. We apply our model to conduct the first continuum-scale simulation of secondary ZABs using aqueous $ZnCl_2$–NH_4Cl as electrolyte. We first use our model to interpret the results of two recent experimental studies of neutral ZABs, showing that the stability of the pH value is a significant factor in cell performance. We then optimize the composition of the electrolyte and the design of the cell considering factors including pH stability, final discharge product, and overall energy density. Our simulations predict that the effectiveness of the pH buffer is limited by slow mass transport and that chlorine-containing solids may precipitate in addition to ZnO.

Introduction

Zinc–air batteries (ZABs) are promising candidates for next-generation energy storage. They offer a high theoretical specific energy (1086 Wh kg_{ZnO}^{-1}) and energy density (6093 Wh L_{ZnO}^{-1}), use abundant and non-hazardous materials, and have superior operational safety characteristics. In fact, primary ZABs using alkaline aqueous KOH electrolytes are already widely utilized for low-current commercial applications such as hearing aids. Unfortunately, the electrical rechargeability and calendar life of these cells are limited. When operated in air, dissolved CO_2 reacts with OH^- to produce CO_3^{2-}. This reaction reduces the ionic conductivity of the electrolyte and slows down the cell reactions.[1] Furthermore, inhomogeneous zinc dissolution and dendritic deposition cause the Zn electrode to change shape and severely limit the cycle life of the cell.[2] Improving the cycling stability of zinc batteries is currently a widely researched topic.[3–11] Aqueous electrolytes with near-neutral pH values were proposed[12–14] as a possible solution to this challenge, and the first steps towards commercialization have been taken.

Aqueous $ZnSO_4$ and $ZnCl_2$ electrolytes are commonly used in industrial zinc electroplating processes. As weakly acidic solutions, the coulombic efficiency of Zn electrodeposition in these electrolytes is nearly 100%.[15] Considering in addition their high electrical conductivity, sulfate- and chloride-based electrolytes are favorable for secondary-zinc-battery applications. Experimental studies show that zinc batteries based on these electrolytes can be reliably operated over hundreds or even thousands of cycles.[13,14,16–18] However, to keep the pH value of the electrolyte in the near-neutral regime, a buffer solution is required to counteract the effects of the oxygen-reduction and oxygen-evolution reactions. In the case of $ZnCl_2$, this is accomplished by the addition of NH_4Cl and NH_4OH. The state of the aqueous zinc ion in buffered electrolytes and the solubility of solid precipitates in the near-neutral pH regime is very complex.[15,19–21] A thorough understanding of the composition of the electrolyte and its behavior during cell operation is necessary to develop a feasible battery. In this paper, we develop a framework for modeling the performance of buffered aqueous electrolytes in zinc batteries and apply it to the $ZnCl_2$–NH_4Cl system.

$ZnCl_2$–NH_4Cl has a long history in commercial electrochemical systems, dating back to the 19th century as the standard electrolyte for zinc–carbon (or so-called Leclanché) batteries.[19,22] These batteries consist of a zinc metal anode and a MnO_2/carbon-paste cathode. Because of their low cost and reliability, non-alkaline zinc–carbon batteries held a significant market share well into the 20th century. A major topic of research in the development of Leclanché batteries is the impact of electrolyte composition on performance and capacity. It is

[a] S. Clark, Prof. Dr. A. Latz, Dr. B. Horstmann
German Aerospace Center (DLR)
Pfaffenwaldring 38–40, 70569 Stuttgart (Germany)
E-mail: birger.horstmann@dlr.de

[b] S. Clark, Prof. Dr. A. Latz, Dr. B. Horstmann
Helmholtz Institute Ulm (HIU)
Helmholtzstr. 11, 89081 Ulm (Germany)

[c] Prof. Dr. A. Latz
Ulm University (UUlm)
Albert-Einstein-Allee 47, 89081 Ulm (Germany)

Supporting Information and the ORCID identification number(s) for the author(s) of this article can be found under https://doi.org/10.1002/cssc.201701468.

commonly noted in the literature that for low NH_4Cl concentrations (e.g., less than 10 wt%) the discharge product is amorphous zinc chloride hydroxide monohydrate (simonkolleite, $ZnCl_2{\cdot}4\,Zn(OH)_2{\cdot}H_2O$) whereas for higher NH_4Cl concentrations the solid product is crystalline zinc diammine chloride ($ZnCl_2{\cdot}2\,NH_3$).[23–25] Furthermore, it is suggested that because of its crystallization morphology, $ZnCl_2{\cdot}2\,NH_3$ poses a higher risk of passivation than $ZnCl_2{\cdot}4\,Zn(OH)_2{\cdot}H_2O$.[26] Unlike alkaline zinc batteries, there is not a standard formulation for the Leclanché electrolyte. The $ZnCl_2/NH_4Cl$ ratio of the electrolyte is adjusted based on the application of the battery.[26] In today's zinc–carbon batteries, $ZnCl_2$–NH_4Cl has mostly been abandoned in favor of KOH because of its high conductivity.

The ongoing search for post-lithium electrochemical energy storage technologies has revived interest in neutral zinc–air batteries. The cheap and non-hazardous materials on which this battery is based, combined with the possibility to achieve a high energy density, make this system a promising contender for sustainable stationary energy storage. The first application of $ZnCl_2$–NH_4Cl in zinc–air batteries was published by Jindra et al. in 1973.[12] They found that a low OH^- concentration in the electrolyte eliminates the formation of carbonates, potentially extending the calendar life of the cell. Nonetheless, the cycling stability was poor. In 2014, Goh, et al.[13] investigated the use of additives such as polyethylene glycol (PEG) and thiourea to improve the homogeneity of zinc electrodeposition. Their cell could be operated continuously for over 1000 h and achieved around 100 cycles. A neutral ZAB developed by Sumboja et al. in 2016 was operated continuously for over 2000 h and achieved around 500 cycles.[14] Although each of these groups has highlighted the importance of the electrolyte composition for optimizing cell performance, there is currently no theoretical analysis of zinc–air batteries using buffered aqueous electrolytes.

Figure 1 shows an operational schematic of a ZAB with $ZnCl_2$–NH_4Cl electrolyte. The battery consists of a metallic Zn electrode and a porous gas-diffusion electrode (GDE) loaded with a bifunctional air catalyst. MnO_2 is the most commonly used non-precious metal catalyst.[17,27] The liquid electrolyte separates the electrodes and conducts ions across the cell. Depending on the distance between the electrodes, this region may or may not contain a porous separator to prevent an internal short circuit.

When the cell is discharged, the metallic Zn electrode dissolves and forms aqueous Zn^{2+} ions, which can then form complexes with other species in solution [Eq. (1)],

$$Zn \rightleftharpoons Zn^{2+} + 2\,e^-, \quad E^0 = -0.762\,V \tag{1}$$

The exact composition of these zinc complexes is highly sensitive to the conditions in the electrolyte and will be discussed in detail in the following sections. When the solubility limit of zinc is reached, various solid products including ZnO, $Zn(OH)_2$, $ZnCl_2{\cdot}4\,Zn(OH)_2{\cdot}H_2O$, and $ZnCl_2{\cdot}2\,NH_3$ can precipitate. At the GDE, the oxygen reduction reaction (ORR) consumes dissolved O_2 and H^+ and produces H_2O [Eq. (2)],

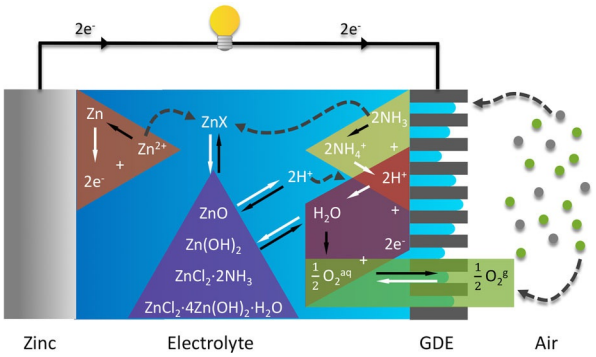

Figure 1. Operational diagram of a zinc–air battery with $ZnCl_2$–NH_4Cl electrolyte. The colors show the various (electro)chemical reactions in the cell; the shapes have no special meaning. The white arrows indicate the direction of these reactions during discharging; the black arrows indicate the direction during charging. The dashed arrows show important transport pathways. Gaseous oxygen molecules enter the cell through the GDE and dissolve in the electrolyte (green). Dissolved oxygen molecules in the GDE are reduced with the help of a bifunctional catalyst and react with H^+ to form H_2O (red). The loss of H^+ disturbs the equilibrium of the NH_4^+/NH_3 species, and the buffer reaction stabilizes the pH value in the GDE (yellow). The metallic Zn electrode dissolves to form aqueous zinc ions, which can then form complexes with NH_3 and Cl^- (orange). Based on the local pH value and concentrations of Zn^{2+}, NH_3, and Cl^-, a variety of solid discharge products may precipitate (purple). ZnO is the most desirable product, and chlorine-containing solids are least desirable.

$$0.5\,O_2{}^{aq} + 2\,H^+ + 2\,e^- \rightleftharpoons H_2O, \quad E^0 = 1.229\,V \tag{2}$$

There is a tendency for the electrolyte to become alkaline because of the loss of H^+. However, the weakly acidic nature of the electrolyte acts as a pH buffer [Eqs. (3) and (4)],

$$NH_4{}^+ \rightleftharpoons NH_3 + H^+, \text{ and} \tag{3}$$

$$Zn^{2+} + n\,NH_3 \rightleftharpoons Zn(NH_3)_n{}^{2+}, \tag{4}$$

which stabilizes the pH value in the neutral regime.

It is important to note that the ability of the electrolyte to stabilize the pH value in the neutral range is attributable to the interactions between $ZnCl_2$ and NH_4Cl. The equivalence point of the NH_4^+/NH_3 buffer[28] is at pH 9.8. A solution containing only NH_4Cl would stabilize the pH value for a short time, but the electrolyte would quickly become alkaline as the concentration of NH_3 increases. When NH_4Cl is mixed with $ZnCl_2$, Zn^{2+} ions form complexes with the NH_3 in solution, which are stable in the in pH range of roughly 6–10. By providing a means to take up free NH_3, the presence of these zinc–ammine complexes increases the capacity of the buffer solution in the neutral range.

When the cell is charged, the oxygen evolution reaction (OER) consumes H_2O and produces $O_2{}^{aq}$ and H^+ at the GDE. Zn^{2+} is deposited from its aqueous forms at the Zn electrode. Again, the buffer reactions stabilize the pH value in the near-neutral domain. As zinc is redeposited from its aqueous state, the concentration decreases to a point below its saturation concentration and the solid precipitates dissolve.

Previous studies simulated ZABs with alkaline KOH electrolytes.[1,29–32] Although much of the same methodology may be applied to ZABs with neutral electrolytes, there is one significant gap. The strongly alkaline composition of standard roughly 30 wt% KOH electrolytes helps maintain a constant pH value during operation. As a result, the thermodynamic stability of the dominant aqueous zinc species ($Zn(OH)_4^{2-}$) also remains constant. Other investigations[20,21] of the thermodynamic stability of zinc–ligand complexes in $ZnCl_2$–NH_3Cl show that within the near-neutral pH domain even slight changes in the pH value can induce significant shifts in the dominant zinc complex. This, in turn, influences both the physicochemical properties and the buffering capacity of the electrolyte. Therefore, a dynamic cell-level model of a ZAB with a near-neutral electrolyte should also consider the coupled effects of pH value and aqueous zinc concentration. Our quasiparticle approach makes this possible.

In this work, we present the first mathematical model of zinc–air batteries with aqueous $ZnCl_2$–NH_4Cl electrolytes. In the following sections, we discuss the thermodynamic basis for our model (electrolyte equilibrium thermodynamics) and present a new method for modeling buffered aqueous electrolytes (quasiparticle model). We provide an overview of the parameters and conditions implemented in the model (computational details) and discuss the predictions of the resulting simulations (results and discussion). We compare the results of our simulations with existing experimental measurements, perform an initial optimization of the ZAB cell, and suggest topics for further research.

Model Development and Application

Electrolyte equilibrium thermodynamics

In this section, the equilibrium thermodynamics of aqueous $ZnCl_2$–NH_4Cl solution is discussed. A framework for the thermodynamic model of this system was already laid out in existing works.[20,21]

The first step in modeling the dynamic behavior of $ZnCl_2$–NH_4Cl was to understand its equilibrium composition. In the electrolyte, zinc may exist as either free Zn^{2+} ions or zinc–ligand complexes. Within the near-neutral pH range, the stability of the aqueous zinc–ligand complexes is very sensitive to changes in the electrolyte environment.[19–21,33] Understanding the coupled effects between the formation of these complexes and electrolyte pH value is essential to interpret the performance of the ZAB. To predict this behavior, we developed a thermodynamic model of aqueous $ZnCl_2$–NH_4Cl in the near-neutral pH domain.

Our model considered a total of 16 aqueous species. These included elementary species (H^+, OH^-, Zn^{2+}, Cl^-, NH_4^+, and NH_3), zinc–chloride complexes ($ZnCl^+$, $ZnCl_2$, $ZnCl_3^-$, and $ZnCl_4^{2-}$), zinc–ammine complexes ($Zn(NH_3)^{2+}$, $Zn(NH_3)_2^{2+}$, $Zn(NH_3)_3^{2+}$, and $Zn(NH_3)_4^{2+}$), and ternary zinc complexes ($ZnCl_3(NH_3)^-$ and $ZnCl(NH_3)_3^+$). Additionally, four solid discharge products were possible in the model: ZnO, $Zn(OH)_2$, $ZnCl_2{\cdot}4\,Zn(OH)_2{\cdot}H_2O$, and $ZnCl_2{\cdot}2\,NH_3$.

The homogeneous electrolyte reactions and their corresponding thermodynamic equilibrium constants[20,21,28] are summarized in Table 1. According to the law of mass action, for a system at constant temperature the value of the equilibrium quotient is constant. For example, the equilibrium quotient of the $ZnCl_4^{2-}$ reaction is expressed as $\frac{[ZnCl_4^{2-}]}{[Zn^{2+}][Cl^-]^4} = \beta$, where $\beta = 10^{0.30}$. In this notation, square brackets are used to denote concentrations ($[X] = c_X$) in mol L^{-1}. Using these equilibrium expressions, the concentration of any aqueous species can be expressed in terms of its stability constant and a combination of Zn^{2+}, Cl^-, and NH_3.

Table 1. Homogeneous reactions in the electrolyte and the corresponding thermodynamic stability constants[20,21,28] for ionic strengths 2–8.

Reaction	$\log_{10}\beta$
$Zn^{2+} + Cl^- \rightleftarrows ZnCl^+$	0.10
$Zn^{2+} + 2\,Cl^- \rightleftarrows ZnCl_2$	0.06
$Zn^{2+} + 3\,Cl^- \rightleftarrows ZnCl_3^-$	0.10
$Zn^{2+} + 4\,Cl^- \rightleftarrows ZnCl_4^{2-}$	0.30
$Zn^{2+} + NH_3 \rightleftarrows Zn(NH_3)^{2+}$	2.38
$Zn^{2+} + 2\,NH_3 \rightleftarrows Zn(NH_3)_2^{2+}$	4.88
$Zn^{2+} + 3\,NH_3 \rightleftarrows Zn(NH_3)_3^{2+}$	7.43
$Zn^{2+} + 4\,NH_3 \rightleftarrows Zn(NH_3)_4^{2+}$	9.65
$Zn^{2+} + 3\,Cl^- + NH_3 \rightleftarrows ZnCl_3(NH_3)^-$	3.15
$Zn^{2+} + Cl^- + 3\,NH_3 \rightleftarrows ZnCl(NH_3)_3^+$	7.90
$NH_3 + H^+ \rightleftarrows NH_4^+$	9.80
$OH^- + H^+ \rightleftarrows H_2O$	13.96

The electrolyte was prepared by adding NH_4OH to an aqueous solution of $ZnCl_2$–NH_4Cl until the desired pH value was achieved. As such, the total amount of chloride, zinc, and nitrogen in the system were known and conserved quantities. They were determined from the weighted sums of the concentrations of the component species. The total (T) chloride and zinc concentrations are expressed as Equations (5) and (6):

$$[Cl]_T = [Cl^-] + \sum_{m=1}^{4} m\,[ZnCl_m^{2-m}] + 3\,[ZnCl_3(NH_3)^-] + [ZnCl(NH_3)_3^+] \quad (5)$$

$$[Zn]_T = [Zn^{2+}] + \sum_{n=1}^{4} [Zn(NH_3)_n^{2+}] + \sum_{m=1}^{4} [ZnCl_m^{2-m}] + [ZnCl_3(NH_3)^-] + [ZnCl(NH_3)_3^+] \quad (6)$$

where m and n describe the stoichiometry of the zinc–chloride and zinc–ammine complexes, respectively. The nitrogen atoms in the system are distributed between ammonium and ammonia. The total amount of ammonia is given by Equation (7):

$$[NH_3]_T = [NH_3] + \sum_{n=1}^{4} n\,[Zn(NH_3)_n^{2+}] + [ZnCl_3(NH_3)^-] + 3\,[ZnCl(NH_3)_3^+] \quad (7)$$

and the total nitrogen content is expressed as Equation (8)

$$[N]_T = [NH_3]_T + [NH_4^+] \quad (8)$$

Finally, the local electroneutrality condition in the system must hold, which gives the following relation [Eq. (9)]:

$$2\,[Zn]_T + [NH_4^+] + [H^+] - [Cl]_T - [OH^-] = 0 \quad (9)$$

Considering the twelve equilibrium expressions in Table 1, the conserved quantities in Equations (5), (6), and (8), and the electroneutrality condition in Equation (9), we had sixteen equations and could solve for the sixteen unknown concentrations in the electrolyte.

Table 2. Solid discharge products with the corresponding thermodynamic solubility products[20,21,34] and theoretical energy densities of a cell with pH 7.

Precipitate	$\log_{10}K_{sp}$	ρ^E [Wh L_{precip}^{-1}]
$ZnCl_2{\cdot}2\,NH_3$	−6.42	303
$ZnCl_2{\cdot}4\,Zn(OH)_2{\cdot}H_2O$	−14.2	948
$Zn(OH)_2$	−17	1782
ZnO	−16.7	6093

When the solubility of zinc in the electrolyte is exceeded, solid products precipitate. These reactions reduce the total zinc, chloride, and nitrogen concentrations in the liquid phase, and the formation of solid products plays a decisive role in the performance of the ZAB. Table 2 lists the various solid discharge products considered in our model, their thermodynamic solubility products and theoretical energy densities as the final discharge products of a neutral ZAB. To incorporate the effects of precipitation into our model, we expressed the solubility, for example of $ZnCl_2{\cdot}2\,NH_3$, as $[Zn^{2+}][Cl^-]^2[NH_3]^2 = K_{sp}$, where the solubility product constant $K_{sp} = 10^{-6.42}$ $(mol\,L^{-1})^5$ and the concentrations are in $mol\,L^{-1}$.

The final discharge product in ZABs should be ZnO. It is well documented that the product of zinc batteries with $ZnCl_2$–NH_4Cl electrolyte is either $ZnCl_2{\cdot}2\,NH_3$ or $ZnCl_2{\cdot}4\,Zn(OH)_2{\cdot}H_2O$, depending on the pH value and $ZnCl_2/NH_4Cl$ ratio.[23–26,33,35,36] The precipitation of these products presents two main challenges for cell design: they consume chloride from the electrolyte and they have molar volumes that are significantly larger than zinc metal.

The molar volume of the precipitates has two effects on cell performance: it reduces the overall energy density of the battery and it can contribute to the flooding of the GDE. The theoretical energy density of a ZAB based on each of the final discharge products was calculated as Equation (10):

$$\rho_p^E = 2F\frac{U_{OC}}{V} \tag{10}$$

where U_{OC} is the open-circuit voltage of the cell [V], F is the Faraday constant [$Ah\,mol^{-1}$], and V is the molar volume of the solid product and consumed electrolyte [$L\,mol^{-1}$]. The ZAB was assumed to be rigid with a fixed volume. Volume expansion caused by the precipitation of these solids forces electrolyte into the GDE and degrades the performance of the cell. The loss of chloride causes the ionic conductivity of the electrolyte to decrease.

Using the model described above, we determined the equilibrium composition of the electrolyte and the zinc solubility given the initial formulation.

Quasiparticle model

We present a method for modeling the dynamic behavior of buffered aqueous electrolytes. The following derivation is geared towards readers active in modeling and simulation. Experimentally inclined readers may wish to continue to the section on computational details.

A method of modeling electrolyte transport on the continuum scale was already derived and validated.[1,37–45] An overview of this method applied to ZABs is provided in the Supporting Information. The transport of solutes in the electrolyte was derived from non-equilibrium thermodynamics[1] and can be expressed in generic terms by the mass-continuity equation [Eq. (11)],

$$\frac{\partial(c_i\varepsilon_e)}{\partial t} = -\vec{\nabla}\cdot\left(\vec{N}_i^{DM}\right) - \vec{\nabla}\cdot\left(\vec{N}_i^{C}\right) + \dot{s}_i \tag{11}$$

(where t is time, ε_e is the volume fraction of the electrolyte, $\vec{N}_i^{DM}$ is the diffusion–migration flux, $\vec{N}_i^{C}$ is the convection flux and $\dot{s}_i$ is the source term) and the charge-continuity equation [Eq. (12)],

$$0 = -\vec{\nabla}\cdot\vec{j} + \sum_i z_i\dot{s}_i \tag{12}$$

(where $\vec{j}$ is the electrolyte current density and z_i is the charge number of the solute).

Transport in strongly acidic or basic electrolytes is driven only by heterogeneous chemical reactions, such as those shown in Tables 3 and 4; thus, the continuity equations described above can be easily solved. However, in buffered neutral electrolytes, homogeneous electrolyte reactions can cause the concentrations of individual solutes to shift by orders of magnitude, as shown in the previous section. The enormous changes in concentration make a numerical solution for the continuity equations infeasible. Our quasiparticle framework addressed this challenge. By defining a set of quasiparticles that described the conserved quantities of the homogeneous reactions, we were able to easily solve the continuity equations and determine the state of the electrolyte under dynamic conditions.

Table 3. Fundamental reactions of the zinc–air cell.

Reaction	E^0 [V]
$Zn \rightleftarrows Zn^{2+} + 2\,e^-$	−0.762
$0.5\,O_2(aq) + 2\,H^+ + 2\,e^- \rightleftarrows H_2O$	1.229
$O_2(g) \rightleftarrows O_2(aq)$	–

Table 4. Precipitation reactions in $ZnCl_2$–NH_4Cl.

Reaction
$Zn^{2+} + 2\,Cl^- + 2\,NH_3 \rightleftarrows ZnCl_2{\cdot}2\,NH_3(s)$
$5\,Zn^{2+} + 2\,Cl^- + 9\,H_2O \rightleftarrows ZnCl_2{\cdot}4\,Zn(OH)_2{\cdot}H_2O(s) + 8\,H^+$
$Zn^{2+} + 2\,H_2O \rightleftarrows Zn(OH)_2(s) + 2\,H^+$
$Zn^{2+} + H_2O \rightleftarrows ZnO(s) + 2\,H^+$

Generic form

Please note that the quasiparticles represent quantities that are conserved in the homogeneous reactions. The concentration of the quasiparticles (c_q) can be defined in terms of the concentrations of its constituent components [Eq. (13)]

$$c_q = \sum_i \tau_{i,q}c_i \tag{13}$$

where $\tau_{i,q}$ describes the stoichiometry of the solute i in the quasiparticle q and may take on values $\tau_{i,q} \in Z$.

The homogeneous electrolyte reactions are listed in Table 1. The solute source term attributable to these reactions ($\dot{s}_i^h$) was defined as Equation (14)

$$\dot{s}_i^{h} = \sum_r \tilde{k}_r^{h} \nu_{i,r} \tag{14}$$

where $\tilde{k}_r^{h}$ is the rate of the homogeneous reaction r and $\nu_{i,r}$ is the stoichiometric coefficient of the solute i in the reaction r. Using the stoichiometric coefficient for the quasiparticle ($\tau_{i,q}$), the solute source term was converted into a source term for the quasiparticles [Eq. (15)]:

$$\dot{s}_q^{h} = \sum_{i,r} \tilde{k}_r^{h} \nu_{i,r} \tau_{i,q} \tag{15}$$

We demanded that the relation $\sum_i \nu_{i,r} \tau_{i,q} = 0$ holds, such that for any $\tilde{k}_r^{h}$ Equation (16) was valid:

$$\dot{s}_q^{h} = 0 \tag{16}$$

Thus, the homogeneous reactions do not contribute to the quasiparticle source term.

Mathematically speaking, the quasiparticles were defined such that the vectors $\vec{\tau}_i = \sum_q \tau_{i,q} \vec{e}_q$ spanned the kernel of the matrix ν^T. Considering that the electrolyte is locally charge neutral, the number of quasiparticles needed to describe the system (n_q) is given by the difference of the number of solutes (n_s) and the number of homogeneous reactions (n_{hr}), $n_q = n_s - n_{hr} - 1$.

By assuming that the kinetics of the homogenous electrolyte reactions are fast, we calculated all individual solute concentrations from a few quasiparticle concentrations. The transport of the quasiparticles is determined by the transport of their individual constituents, assuming that the homogeneous reactions occur very quickly. Therefore, the diffusion–migration flux for quasiparticle q becomes Equation (17):

$$\vec{N}_q^{DM} = \sum_i \tau_{i,q} \vec{N}_i^{DM} = \varepsilon_e^{\beta} \sum_i \left(\tau_{i,q} D_i \vec{\nabla} c_i \right) + \sum_i \left(\tau_{i,q} \frac{t_i}{z_i F} \right) \vec{j} \tag{17}$$

where β is the Bruggeman coefficient, D_i is the diffusion coefficient, z_i is the charge number, and t_i is the transference number of the solute. The convective flux of quasiparticle q is defined by Equation (18):

$$\vec{N}_q^{C} = \varepsilon_e^{\beta} c_q \vec{v}_e \tag{18}$$

where $\vec{v}_e$ is the center-of-mass velocity of the electrolyte. How the electrolyte equation of state and current-density equation are derived can be found in the Supporting Information. Now the transport equations for the quasiparticles can be expressed as

$$\frac{\partial (c_q \varepsilon_e)}{\partial t} = -\vec{\nabla} \cdot \left[\varepsilon_e^{\beta} \sum_i \left(\tau_{i,q} D_i \vec{\nabla} c_i \right) + \sum_i \left(\tau_{i,q} \frac{t_i}{z_i F} \right) \vec{j} \right] - \vec{\nabla} \cdot \left(\varepsilon_e^{\tilde{\beta}} c_q \vec{v}_e \right) + \dot{s}_q^{e,p} \tag{19}$$

$$0 = -\vec{\nabla} \cdot \vec{j} + \sum z_i \dot{s}_i^{e} \tag{20}$$

where $\dot{s}_q^{e,p}$ is the source term due to the combined electrochemical and precipitation reactions, and $\dot{s}_i^{e}$ is the source term due to the electrochemical reactions.

Because charge is conserved in the homogeneous reactions, they do not contribute to the electroneutrality equation. Our quasiparticle formulation provides a simple method for modeling a series of coupled chemical reactions taking advantage of the conservation of atom numbers and charge. In the next section, we applied this model to the $ZnCl_2$–NH_4Cl system.

Quasiparticle framework in the $ZnCl_2$–NH_4Cl system

The $ZnCl_2$–NH_4Cl system consists of 16 solutes spanning 12 homogeneous reactions. Therefore, three quasiparticles were needed. To describe the quantities conserved in the homogeneous electrolyte reactions, we defined the following quasiparticles: ammonia ($\widetilde{NH_3}$), ammonium ($\widetilde{NH_4}$), and zinc ($\widetilde{Zn}$). According to the definition in Equation (13), the concentrations of the ammonia and zinc quasiparticles are expressed as Equation (21)

$$\left[\widetilde{NH_3}\right] = [NH_3] + \sum_{n=1}^{4} n[Zn(NH_3)_n^{2+}] + [ZnCl_3(NH_3)^-] + 3[ZnCl(NH_3)_3^+] - [H^+] + [OH^-] \tag{21}$$

and Equation (22)

$$[\widetilde{Zn}] = [Zn^{2+}] + \sum_{n=1}^{4} [Zn(NH_3)_n^{2+}] + \sum_{m=1}^{4} [ZnCl_m^{2-m}] + [ZnCl_3(NH_3)^-] + [ZnCl(NH_3)_3^+] \tag{22}$$

The concentration of the ammonium quasiparticle is expressed as Equation (23):

$$\left[\widetilde{NH_4}\right] = \left[NH_4^+\right] + [H^+] - [OH^-] \tag{23}$$

The sum of $\widetilde{NH_4}$ and $\widetilde{NH_3}$ gives the total concentration of nitrogen [Eq. (24)] whereas the total chloride concentration [Eq. (26)] is expressed by a combination of $\widetilde{NH_4}$ and $\widetilde{Zn}$, assuming local electroneutrality. The total zinc concentration is given by $\widetilde{Zn}$ [Eq. (25)].

$$[N]_T = \left[\widetilde{NH_3}\right] + \left[\widetilde{NH_4}\right] \tag{24}$$

$$[Zn]_T = [\widetilde{Zn}] \tag{25}$$

$$[Cl]_T = 2\left[\widetilde{Zn}\right] + \left[\widetilde{NH_4}\right] \tag{26}$$

Table 5. Reactions that contribute to the quasiparticle source terms.

Reaction
$Zn \rightleftharpoons \widetilde{Zn} + 2e^-$
$\frac{1}{2}O_2(aq) + 2\widetilde{NH_4} + 2e^- \rightleftharpoons 2\widetilde{NH_3} + H_2O$
$5\widetilde{Zn} + 8\widetilde{NH_3} + 9H_2O \rightleftharpoons 8\widetilde{NH_4} + ZnCl_2 \cdot 4Zn(OH)_2 \cdot H_2O(s)$
$\widetilde{Zn} + 2\widetilde{NH_3} \rightleftharpoons ZnCl_2 \cdot 2NH_3(s)$
$\widetilde{Zn} + 2\widetilde{NH_3} + 2H_2O \rightleftharpoons 2\widetilde{NH_4} + Zn(OH)_2(s)$
$\widetilde{Zn} + 2\widetilde{NH_3} + H_2O \rightleftharpoons 2\widetilde{NH_4} + ZnO(s)$

We defined quasiparticles such that the homogeneous reactions do not contribute to the quasiparticle source term [as shown in Eq. (16)]. The source term is instead governed by the electrochemical and precipitation reactions listed in Tables 3 and 4. We rewrote the stoichiometric equations for these reactions to reflect the quasiparticle definitions, as shown in Table 5.

To solve the system, we defined the initial pH value and the total chloride and total zinc concentrations of the system. The concentration of the quasiparticles are given by the mass and charge-continuity equations [Eqs. (19) and (20)], and we used Equations (24), (25), and (26) to solve for $[Zn^{2+}]$, $[Cl^-]$, and $[NH_3]$. With these quantities, the concentrations of all 16 aqueous solutes and the volume fractions of the four solids could be determined.

Computational details

In this section, we discuss the computational details of our model, including the initial conditions and loads used for the simulations. More information on this topic, as well as a complete list of the physical, chemical, and numerical parameters[13,14,20,21,27,28,42,43,46–61] implemented in the model, is presented in greater detail in the Supporting Information.

Model implementation

Our ZAB model consisted of a system of 13 equations: 5 solid-volume-conservation equations, 4 mass-continuity equations, 1 charge-continuity expression, 1 electrolyte-mass-continuity equation, 1 electrolyte-pressure equation of state, and 1 galvanostatic expression. A complete list of the equations is available in the Supporting Information. A 1D finite volume model was developed in MATLAB to implement the theory described above. The mesh was generated with fixed compartment sizes in the Zn electrode and GDE and a variable cell size in the separator. The system of equations was solved using the ode15i solver, a fully implicit solver for differential and algebraic equations.

The computational domain of the ZAB model consisted of the Zn electrode, separator, and GDE. The domain began at the Zn electrode current collector ($x=0$) and ended at the GDE current collector ($x=L_{cell}$), where L_{cell} is the total thickness of the cell.

Simulation conditions

Our first full-cell simulation was based on the ZAB developed by Goh et al.[13] The electrolyte was 0.51 M $ZnCl_2$–2.34 M NH_4Cl with the pH value adjusted to 6 through the addition of NH_4OH. For simplicity, this electrolyte is referred to in the text as Electrolyte A. The anode was a polished zinc foil with a thickness of 0.5 mm, and the cathode was a carbon GDE loaded with 4.5 mg cm^{-2} MnO_2 as catalyst. The Zn electrode and the GDE were 30 mm apart and separated by an electrolyte bath. The cell was discharged at 5 mA cm^{-2} for 4 h and charged at 2.5 mA cm^{-2} for 8 h. This cell is referred to in the text as Cell A.

Our second full-cell simulation was based on the work of Sumboja et al.[14] The electrolyte was 0.26 M $ZnCl_2$–5 M NH_4Cl with the pH value adjusted to 7. This electrolyte is referred to in the text as Electrolyte B. The anode was a polished zinc foil with a thickness of 0.5 mm, and the cathode was a carbon GDE loaded with 4.5 mg cm^{-2} MnO_2. The electrodes were 24 mm apart and separated by an electrolyte bath. The cell was discharged at 1 mA cm^{-2} for 2 h and charged at 1 mA cm^{-2} for 2 h. This cell is referred to in the text as Cell B.

Finally, we performed a series of simulations in which the electrolyte composition and cell architecture were adjusted to represent a feasible battery. Simulations were carried out to optimize the separator thickness, electrolyte composition, and the architecture of the Zn electrode. The performance of these cells was rated according to pH stability, composition of the discharge product, and the overall energy density of the battery. The optimization simulations were performed under galvanostatic conditions with a charge–discharge current density of 1 mA cm^{-2}.

Results and Discussion

In this section, we present the results of our simulations and discuss the significant findings. We begin by considering the equilibrium composition of the electrolyte and its dependence on the pH value and zinc and chloride concentration. We continue by analyzing the galvanostatic cycling performance of Cell A and compare it with the modifications introduced in Cell B. Finally, we present an optimization of cell performance based on cell design and electrolyte composition and discuss important aspects for future development.

Electrolyte composition

The composition of aqueous $ZnCl_2$–NH_4Cl strongly depends on the total zinc and chloride concentrations as well as on the pH value of the solution.

Figure 2 shows the distribution of zinc–ligand complexes for a system of constant total zinc and chloride concentrations

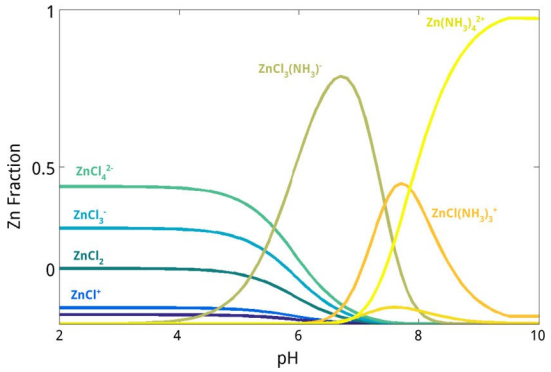

Figure 2. Aqueous zinc complex distribution vs. pH value for 0.51 M $ZnCl_2$–2.34 M NH_4Cl electrolyte. At acidic pH values, low NH_3 concentrations cause the solution to be dominated by zinc–chloride complexes. As the pH increases, more NH_3 becomes available, leading first to mixed complexes in the near-neutral domain and finally to the dominance of zinc–ammine complexes.

with variations in the pH value. At low pH values, the concentration of NH_3 in solution is very low. As a result, Zn^{2+} tends to form complexes with Cl^- ions. As the pH value of the system increases, NH_4^+ begins to dissociate and more NH_3 becomes available. In the neutral pH range, ternary zinc–chloride–ammonia complexes dominate. Finally, NH_3 is available in significant quantities and zinc–ammine complexes ($Zn(NH_3)_4^{2+}$) dominate.

The buffering effect in the near-neutral pH range is determined by the formation of zinc–ammine complexes. As a weak acid, NH_4Cl acts as a pH buffer on its own, $NH_4^+ \rightleftarrows NH_3 + H^+$. But as the concentration of NH_3 in the solution increases, the reaction approaches its equivalence point and the pH becomes alkaline. By taking up excess NH_3, the zinc–ammine complexes allow the $NH_4^+ \rightleftarrows NH_3 + H^+$ reaction to act as a proton source while keeping the concentration of free NH_3 relatively low. As shown in Figure 2, the zinc–ammine complexes stabilize the pH value in the range between circa 6 (where $ZnCl_3(NH_3)^-$ begins to dominate) and circa 9.8 (where the NH_4^+/NH_3 reaction reaches its equivalence point). This is one of the main reasons why the electrolyte should be a mix of $ZnCl_2$ and NH_4Cl and not a pure solution of one or the other. Figure 3 presents

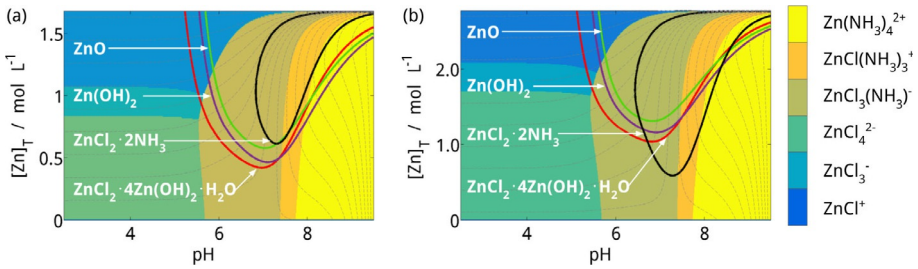

Figure 3. Dominant aqueous zinc complexes and discharge product solubilities for a total chloride concentration of (a) 3.36 mol L^{-1} (Cell A) and (b) 5.54 mol L^{-1} (Cell B). Each colored region of the charts corresponds to the composition of the dominant zinc complex (unit less). The solid lines correspond to the solubility of the various precipitates. The dashed lines show paths of constant nitrogen concentration in the electrolyte.

the thermodynamic stability diagrams of both the zinc–ligand complexes and the solid precipitates for a fixed total chloride concentration while varying the pH value and total zinc concentration. The colored regions correspond to dominant zinc–ligand complexes, the colored lines show the solubilities of the precipitates, and the dashed lines represent paths of constant total nitrogen concentration. Because the total nitrogen concentration is constant (in the absence of precipitation and evaporation), the electrolyte composition will follow the dashed lines as the cell is discharged or charged. For pH values between 6 and 10, zinc can be dissolved without significantly altering the pH value. This represents the buffer effect caused by the uptake of NH_3 by the zinc–ligand complexes.

The precipitates considered in the model are insoluble in the near-neutral pH domain. Consider the system shown in Figure 3a. By locating the initial condition of pH 6 and $[Zn]_T = 0.51$ mol L^{-1} (Electrolyte A) and following the dashed path of constant nitrogen concentration, $ZnCl_2{\cdot}4\,Zn(OH)_2{\cdot}H_2O$ is the first solid to precipitate, followed by $Zn(OH)_2$ and ZnO. The thermodynamically favored solid discharge product can change according to the pH value and the amount of chloride in the electrolyte, as shown in Figure 3b. Starting at the initial conditions pH 7 and $[Zn]_T = 0.26$ mol L^{-1} (Electrolyte B), the path of constant nitrogen concentration leads directly into the region of $ZnCl_2{\cdot}2\,NH_3$ insolubility. Therefore, it is possible to tune the initial composition of the electrolyte to favor the desired discharge product. This shift in the solid product was also noted in experimental investigations of zinc–carbon batteries.[26,36]

Cell operation and experimental validation

Our simulations elucidate the physicochemical processes that occur in the cell during galvanostatic operation. We begin by simulating the performance of neutral ZABs reported in literature. The experimental evaluation of Cell A[13] shows that under the operating conditions considered in the simulation it can be operated for up to 26 full charge–discharge cycles over about 13 days. We investigate the changes in the electrolyte during cycling, compare the simulated cell voltage with the experimental voltage profiles, and predict possible causes of failure. The development of Cell B builds on the progress of Cell A. The experimental investigation[14] shows that the cell can be stable operated for 540 cycles over 90 days. We simulate the design changes introduced in Cell B and consider what effects could be responsible for the gain in lifetime.

First, the basic processes occurring in the ZAB during galvanostatic cycling are investigated. Figure 4a, c, and e show the concentration profiles of zinc, NH_3, and pH value as the cell is discharged. When the discharge of Cell A begins, the metallic Zn electrode is dissolved to form aqueous species, which may exist as either zinc–ligand complexes or solvated Zn^{2+} ions. At the GDE, the ORR consumes H^+, and the $NH_4^+ \rightleftarrows NH_3 + H^+$ reaction (combined with the uptake of NH_3 by the zinc–ligand complexes) stabilizes the electrolyte pH value. Figure 4a shows that at the end of discharge zinc in the GDE exists mostly as complexes with NH_3. Once zinc exists exclusively as $Zn(NH_3)_4^{2+}$, then its capacity to take up excess NH_3 is exhausted and the concentration of NH_3 increases as shown in Figure 4c. When the concentration of NH_3 approaches its equivalence point with NH_4^+, the pH value becomes steadily more alkaline in the GDE, as shown in Figure 4e. At the Zn electrode, the small amount of NH_3 present is taken up by the excess Zn^{2+} ions and the pH value becomes slightly more acidic.

Figure 4b, d, and f show the concentration profiles in the cell during charging. When the cell is charged, aqueous zinc is redeposited at the Zn electrode. At the GDE, the OER produces H^+ and the equilibrium of the $NH_4^+ \rightleftarrows NH_3 + H^+$ reaction moves towards NH_4^+. The NH_3 that had formed complexes with Zn^{2+} during discharge is now released back into the solution to stabilize the equilibrium with NH_4^+. Figure 4b shows that at the end of charging, zinc in the GDE has released all of the available NH_3 and exists exclusively as zinc chloride complexes. Figure 4d shows that during the OER, the concentration of NH_3 in the GDE steadily decreases as it is converted into NH_4^+. Once the NH_3 released from the locally available zinc complexes is exhausted, additional NH_3 must diffuse into the GDE from the separator. However, some of the zinc–ammine complexes produced during discharge diffuse into the bulk electrolyte and they cannot be quickly transported to the GDE. These effects have significant consequences for the pH value in the cell. Because the amount of NH_3 in the GDE is no longer sufficient to convert the H^+ produced by the OER into NH_4^+, the pH value becomes acidic at the end of charging. This effect is shown in Figure 4f. Conversely, the increase in the concentration of NH_3 at the Zn electrode causes the pH value in that region to become slightly more alkaline.

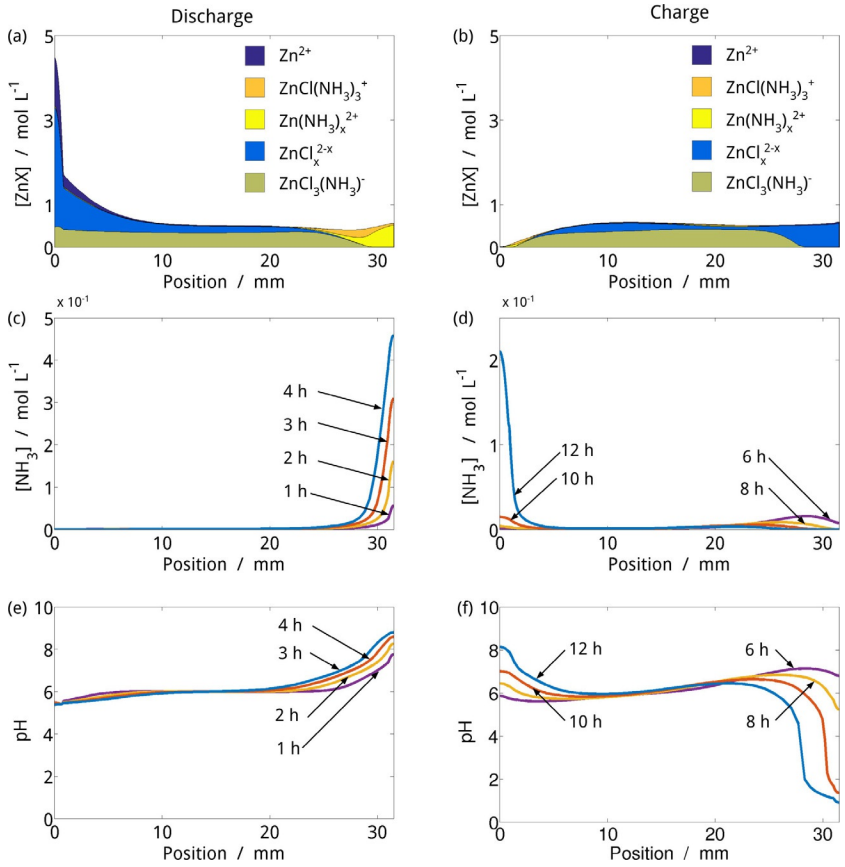

Figure 4. Electrolyte composition in Cell A during discharging and charging. At the end of discharging (a), zinc in the GDE exists as $Zn(NH_3)_4^{2+}$. Once the capacity of zinc to take up NH_3 is completely utilized, NH_3 accumulates in the GDE (c). As the NH_4^+/NH_3 solution approaches its equivalence point, the pH value in the GDE becomes steadily more alkaline (e). At the Zn electrode, the small amount of NH_3 present is taken up by excess Zn^{2+} and the pH value becomes slightly more acidic. When the cell is charged, the production of H^+ in the GDE pushes the equilibrium of the ammonium buffer back towards NH_4^+. The zinc–ammine complexes release NH_3 back to the solution as charging progresses, and at the end of charging, zinc in the GDE exists exclusively as zinc–chloride complexes (b). To stabilize the pH value in the GDE, there must be NH_3 available for the conversion into NH_4^+. However, a considerable amount of the NH_3 produced during discharging diffuses into the bulk electrolyte and cannot be quickly recovered. This leads to a depletion of NH_3 in the GDE (d). At the Zn electrode, the concentration of NH_3 increases because of the redeposition of zinc. Without NH_3 to stabilize the pH value, the electrolyte in the GDE becomes acidic (f). At the Zn electrode, the loss of aqueous Zn^{2+} and the relative excess of NH_3 cause the pH value to increase.

MnO_2 is often used as an OER catalyst in alkaline and neutral solutions, but it is known to be unstable under acidic conditions due to the dissolution of Mn.[62–64] If the pH value in the GDE drops to a value of 1 or below, as occurs during the charging of Cell A (Figure 4 f), the risk of accelerated catalyst degradation is increased.

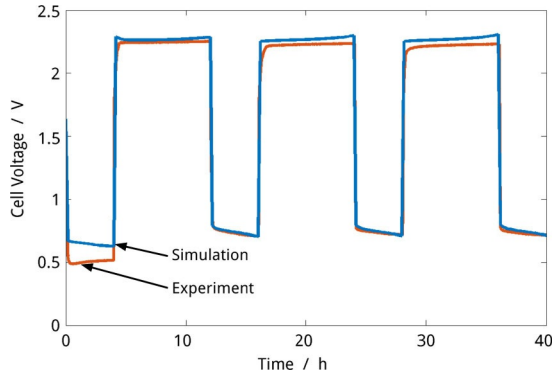

Figure 5. Simulated voltage profile of Cell A over three charge–discharge cycles, compared with experimental results;[13] $j_d = 5\ mA\,cm^{-2}$, $t_d = 4$ h, $j_c = 2.5\ mA\,cm^{-2}$, $t_c = 8$ h.

Figure 5 compares the simulated cell voltage over three cycles with experimental data. During discharge, there is a slight negative slope in the cell potential, which can be attributed to the pH shift in the GDE. Between the first and second discharges there is a positive shift in cell potential. In our model it is circa 100 mV, in the experimental data it is circa 250 mV. This shift in discharge voltage is due partly to the increase in the active surface area of the Zn electrode.

Initially, the Zn electrode is a polished sheet, but when zinc is electrodeposited, it takes on a porous morphology. This leads to an increase in the active surface area of the Zn electrode and a decrease in the overpotential of the electrochemical reaction. Our model considers this effect by altering the pore size of the deposited zinc. More information on this topic is available in the Supporting Information. However, the overpotential of the zinc reaction cannot be solely responsible for a 250 mV voltage shift. There may be other mechanisms (such as activation of the MnO_2 catalyst) occurring simultaneously,

which could increase the magnitude of the voltage shift between the first and second discharge. Further experimental data is required to accurately characterize this effect.

As noted in the previous sections, the final product has a significant effect on cell performance. In the case of Cell A, however, the discharge capacity is rather small and the cell is operated with an excess of electrolyte. Few solids precipitate, and they have little effect on the cell performance.

In summary, Cell A shows that a zinc–air battery can be reliably cycled in the $ZnCl_2$–NH_4Cl electrolyte. However, the shift towards acidic pH values in the GDE can limit the material stability and cell lifetime. Cell B addresses one of these challenges. The results of our simulation are very similar to those in Cell A, with one notable exception: the pH value in Cell B remains in the near-neutral regime when cycled. By avoiding the drop to acidic pH values, the stability of the catalyst and GDE is maintained, and the cell lifetime is improved. The pH profile of the cell at the end of discharge and end of charge are shown in Figure 6.

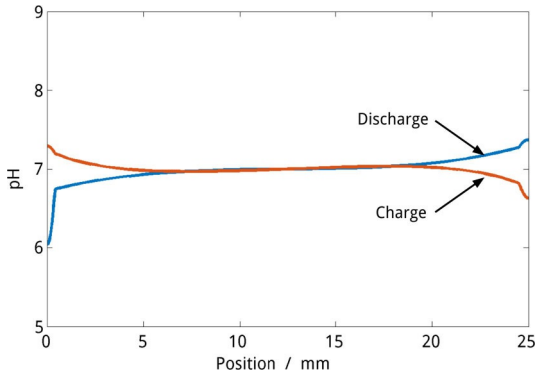

Figure 6. pH profiles of Cell B at the end of the first discharge cycle and end of the first charge cycle.

There are a few factors that contribute to the gain in pH stability. First, Cell B is charged at a lower current density, which reduces the NH_3 concentration gradient and allows more of the capacity of the buffer solution to be utilized. Second, the initial pH value of the electrolyte is 7 instead of 6. That means that initially there is more NH_3 in solution. More importantly, the state of the aqueous zinc ion is dominated by zinc–ammine complexes. As the pH drops to more acidic values, these complexes can release NH_3 to the electrolyte. Third, the separator length is shorter, which reduces the magnitude of the NH_3 concentration gradient and limits the distance NH_3 can diffuse away from the GDE. More information is available in the Supporting Information.

Although Cell B does show a dramatic gain in lifetime and pH stability over Cell A, it is operated at a lower current density and to a shallower depth of discharge (DoD). Our simulations show that the zinc solubility in the electrolyte is barely breached, and few solids precipitate.

Cell B represents another important step towards designing a practical neutral zinc–air cell, but questions remain. In the following simulations we show what happens when the cell is discharged to states at which significant amounts of solids precipitate, and investigate how the electrolyte composition and cell design may be optimized.

Cell-design optimization

The experimental studies modeled in the previous section show the general viability of the neutral electrolyte for secondary zinc–air battery applications. However, these cells are operated at relatively shallow DoDs, thereby avoiding complications that could arise due to the precipitation of chlorine-containing solids.

The precipitation of solids in the zinc–air cell induces a volume expansion, which has the potential to flood the GDE. A means of moderating the electrolyte level is necessary to avoid this effect. In commercial ZAB button cells, a gas void is included in the Zn electrode,[1] which provides room for the electrode to expand during discharge without forcing electrolyte into the GDE. We introduce this mechanism in our model by considering the entire domain of the ZAB to be a porous structure, the saturation of which is calculated using the Leverett approach described in the Supporting Information. The porous structures are initially 40% saturated.

The Zn electrode used in the experimental studies is a polished foil. While this is beneficial for studying the kinetics of the electrochemical reaction, it is impractical for use in a real battery. Commercial ZABs use zinc powder with particles on the order of 100 μm in diameter.[65] This powder may then be mixed with binder and electrolyte to form a paste. We consider a Zn paste electrode for our optimizations. Cells A and B feature a bath of excess electrolyte. This ensures that the cell always has sufficient amounts of electrolyte available, but it can lead to strong concentration gradients, increase the internal resistance of the cell, and lower the overall energy density. It is beneficial to design the cell using a thinner separator.

Figure 7 shows the pH profile across the cell for various separator thicknesses at the end of charging. Reducing the thickness of the separator improves the performance of the battery in three notable ways. First, it reduces the length of the transport paths in the battery, allowing more efficient utilization of NH_3. Second, the reduced volume of the electrolyte accelerates

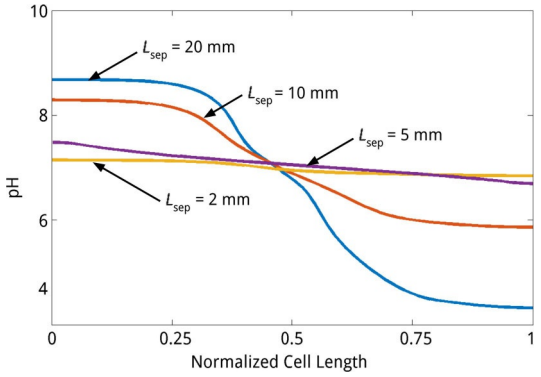

Figure 7. Gradients of the pH value at the end of charging for different separator distances versus the normalized length of the cell.

the precipitation of solids, which stabilizes the buffer solution. Third, the reduction of excess volume increases the energy density of the cell. The simulations show that for low current densities (1 mA cm^{-2}), separator lengths less than 2 mm are sufficient to maintain a stable pH value. As the energy density is inversely proportional to the separator length, we choose a 0.5 mm separator for the remainder of the optimizations.

With the optimum size of the separator defined, we turn our attention to the electrolyte composition. We define a standard test architecture to evaluate the effects of different electrolytes on battery performance. Our standard cell consists of a Zn electrode 5 mm in length, a 0.5 mm separator, and a 0.5 mm GDE. The cell is operated at 1 mA cm^{-2}. We first search for electrolyte compositions that thermodynamically favor the desired discharge product. Then we evaluate the stability of the electrolytes during cell operation.

According to existing studies on zinc–carbon batteries and the thermodynamic analysis presented previously, the thermodynamically favored discharge product in most cases is either $ZnCl_2{\cdot}2\,NH_3$ or $ZnCl_2{\cdot}4\,Zn(OH)_2{\cdot}H_2O$. As these solids precipitate, the aqueous chloride concentration decreases, altering the properties of the electrolyte. For the system to function as a zinc–air battery, the discharge product should be ZnO or alternatively $Zn(OH)_2$.

To predict an electrolyte composition that features a stable chloride concentration in the near-neutral pH regime and precipitates as either ZnO or $Zn(OH)_2$, we revisit the thermodynamic analysis from the section on electrolyte composition. The risk of precipitating chlorine-containing solids increases with increasing the total chloride concentration. For a total chloride concentrations of circa 3 mol L^{-1} and pH values above 7.5, $Zn(OH)_2$ is the thermodynamically favored product. The initial electrolyte composition should be formulated such that it is at the solubility limit of $Zn(OH)_2$ to facilitate precipitation. We therefore propose an electrolyte composition of 0.5 M $ZnCl_2$–1.6 M NH_4Cl with the pH adjusted to 8 (referred to in the text as Electrolyte C). Evaporation of NH_3 through the GDE is not considered in this analysis and should be a topic for further research. More information on this topic is available in the Supporting Information.

We evaluate the performance of Electrolytes A, B, and C by simulating the complete discharge of the test cell architecture to a cut-off voltage of 0.6 V. Figure 8a shows the total volume fractions of solid precipitates in the cell and the total chloride concentration versus discharged capacity, and Figure 8d shows the cell voltage and average pH value in the GDE for Electrolyte A. The discharge occurs in three stages. In the first stage, the total chlorine concentration decreases as $ZnCl_2{\cdot}4\,Zn(OH)_2{\cdot}H_2O$ precipitates. The pH value in the GDE becomes steadily more alkaline. This is because the precipitation of $ZnCl_2{\cdot}4\,Zn(OH)_2{\cdot}H_2O$ only removes 1.6 OH^- for every Zn^{2+} precipitated. In stage 2, the chloride concentration decreases to the lower solubility limit of $ZnCl_2{\cdot}4\,Zn(OH)_2{\cdot}H_2O$ and the dominant discharge product shifts to $Zn(OH)_2$. The pH value in the GDE begins to stabilize, because the precipitation of $Zn(OH)_2$ removes 2 OH^- for every Zn^{2+} precipitated. In the final stage, the capacity of the buffer solution is exhausted and the

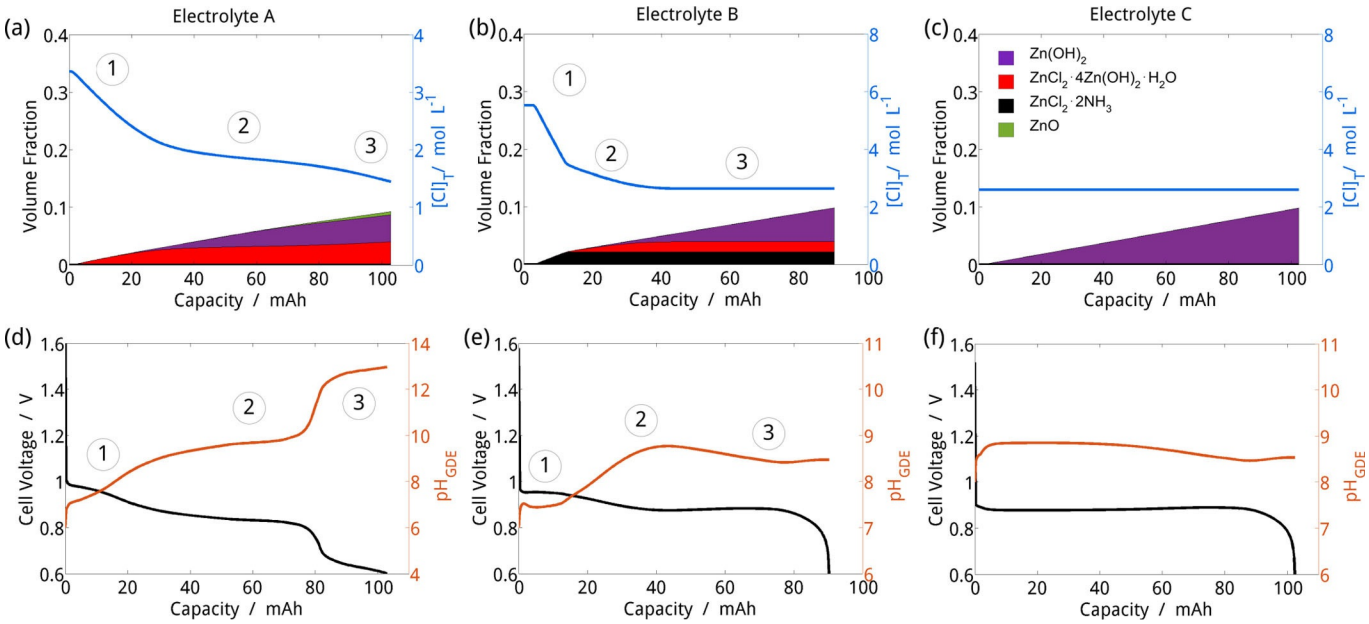

Figure 8. Stability of the total chloride concentration and pH value in ZAB standard test architecture (L_{Zn} = 5 mm) during discharge for various electrolyte compositions. For electrolytes with high initial chloride concentrations (a) and (b), the precipitation of chlorine-containing solids reduces the total chloride concentration until $Zn(OH)_2$ begins to precipitate. By reducing the total chloride concentration and moving to slightly alkaline pH values (c), the discharge product becomes exclusively $Zn(OH)_2$ and the chloride content of the electrolyte is stabilized. The pH stability of the electrolyte is also affected by the discharge product. For electrolytes in which $ZnCl_2{\cdot}4\,Zn/OH)_2{\cdot}H_2O$ precipitation dominates, the buffer solution is not effectively replenished and the pH is unstable (d). The effects of the pH variations can be seen in the cell potential. The precipitation of $ZnCl_2{\cdot}2\,NH_3$ and $Zn(OH)_2$ adequately stabilizes the pH value [(e) and (f)]. For these reasons, ZnO or $Zn(OH)_2$ are the desired discharge products.

pH value in the GDE becomes alkaline. Small amounts of ZnO precipitate.

Figure 8b and e shows the discharge characteristics of a test cell with Electrolyte B. Again, the discharge occurs in three stages. In the first stage, the total chloride concentration decreases rapidly as $ZnCl_2{\cdot}2\,NH_3$ precipitates and the pH value remains stable. The second stage begins when the total chloride concentration is reduced to a level at which $ZnCl_2{\cdot}4\,Zn(OH)_2{\cdot}H_2O$ precipitation is favored. The pH value becomes steadily more alkaline because of insufficient removal of OH^-. In the final stage, the discharge product shifts to $Zn(OH)_2$ and the total chloride concentration and pH value stabilize.

Figure 8c and f shows the discharge characteristics of a test cell using Electrolyte C. The composition of this electrolyte is tuned to favor only $Zn(OH)_2$ precipitation. The results show that both total chloride concentration and pH value remain stable throughout the discharge of the cell. The end of discharge occurs when the Zn electrode is passivated by $Zn(OH)_2$.

The shift in the solid discharge product observed in these simulations can be clarified by re-examining the thermodynamic stability plots in Figure 3. For high chloride concentrations, neutral pH values, and total zinc concentrations less than 1 mol L^{-1}, the battery discharge follows a path that takes it directly into the region of $ZnCl_2{\cdot}2\,NH_3$ insolubility (Figure 3b). When the total chloride concentration in the electrolyte is reduced, as shown in Figure 3a, the dominant discharge product becomes $ZnCl_2{\cdot}4\,Zn(OH)_2{\cdot}H_2O$ for slightly acidic-neutral pH values and $Zn(OH)_2$ for slightly alkaline pH values.

This analysis yields a few significant insights for zinc–air battery design. First, $ZnCl_2{\cdot}2\,NH_3$ and $ZnCl_2{\cdot}4\,Zn(OH)_2{\cdot}H_2O$ are not desirable discharge products. The precipitation of these solids consumes chloride from the electrolyte and reduces the effectiveness of the pH buffer. Second, electrolytes featuring a high initial chloride concentration will eventually converge to a steady-state chloride concentration at or near the solubility limit of $ZnCl_2{\cdot}2\,NH_3$ and $ZnCl_2{\cdot}4\,Zn(OH)_2{\cdot}H_2O$. Therefore, it should be noted that any advantages of high chloride concentration (e.g., improved conductivity) are only valid for shallow discharges. Third, it is possible to tune the initial concentration of the electrolyte to exclusively precipitate $Zn(OH)_2$, as demonstrated by our proposed Electrolyte C composition. Favoring the precipitation of $Zn(OH)_2$ over chlorine-containing solids is a modest improvement for cell operation. However, a means to thermodynamically or kinetically favor ZnO precipitation should be a topic for ongoing research.

Finally, we consider the design of the Zn electrode, which strongly influences the capacity and energy density of the battery. It is well known that passivation caused by the precipitation of solid products on the electrode surface is perhaps the biggest challenge limiting the full utilization of zinc in batteries. In alkaline zinc batteries, a shell of ZnO or $Zn(OH)_2$ forms around the zinc particles.[65] This shell isolates the surface of the zinc particle from the electrolyte and limits the transport of aqueous species to and from the electrode surface. When the thickness of the ZnO shell surpasses a critical value, the resistance to mass transport becomes so great that the concentrations of aqueous species at the zinc surface are depleted and the reaction cannot proceed. When this occurs, the electrode is said to be passivated.

Although this effect has been extensively studied in alkaline electrolytes, there is little research dedicated to the passivation process in the $ZnCl_2$–NH_4Cl system. It is thought that $ZnCl_2{\cdot}2\,NH_3$ is crystalline and dense and therefore presents a high resistance to the transport of solutes between the electrolyte and electrode. On the other hand, $ZnCl_2{\cdot}4\,Zn(OH)_2{\cdot}H_2O$ is amorphous and porous and presents a lower resistance to mass transport.[26] Therefore, it is likely that $ZnCl_2{\cdot}4\,Zn(OH)_2{\cdot}H_2O$ is less passivating than $ZnCl_2{\cdot}2\,NH_3$ and could help achieving a higher zinc utilization in the battery. This should be the subject of a more in-depth study. For the purpose of this optimization, we assume that the zinc particles are spheres with an initial diameter of 100 μm. When the thickness of solid precipitates around the particle exceeds 5 μm, the particle is considered to be passivated.

Figure 9 shows the energy density of zinc–air batteries considering the electrolyte compositions A, B, and C discussed previously. An electrolyte composition that favors ZnO precipitation is not immediately apparent. However, it is commonly noted that $Zn(OH)_2$ can undergo a decomposition to ZnO. Therefore, we evaluate what the performance of a theoretical ideal electrolyte would be, if the precipitation of ZnO were achieved. We set the composition for this idealized electrolyte at 0.5 M $ZnCl_2$–2 M NH_4Cl pH 7 (referred to in the text as Electrolyte D). For this analysis the Zn electrode thicknesses are varied from 0.5 to 20 mm. A cutoff voltage of 0.6 V is used as a reference.

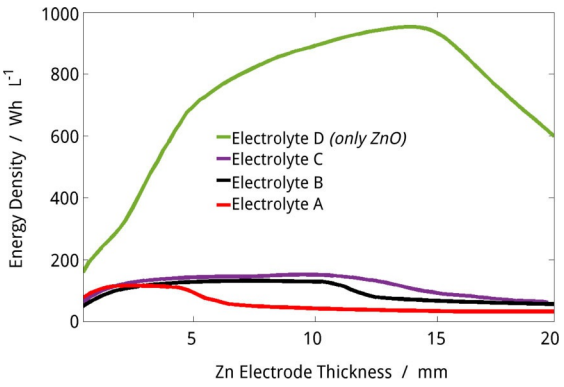

Figure 9. Energy density of the zinc–air cell with various electrolyte compositions versus Zn electrode thickness considering a cutoff voltage of 0.6 V. For thin Zn electrodes, the energy density is limited by the passivation of zinc. For thick Zn electrodes, the pH instability causes a drop in cell voltage.

For small Zn electrodes, solid precipitates accumulate and passivate the electrode quickly. As the size of the electrode increases, the passivation risk becomes less severe and a higher fraction of the zinc is utilized, leading to a higher energy density. For thick Zn electrodes, the long transport path for the aqueous species destabilizes the pH value in the GDE and reduces the energy density and lifetime of the cell. This is strongly the case in Electrolyte A. As shown in Figure 8a, the precipitation of $ZnCl_2{\cdot}4\,Zn(OH)_2{\cdot}H_2O$ cannot stabilize the buffer

solution and the pH value becomes steadily more alkaline. This effect is exacerbated by the longer transport paths of thick Zn electrodes. The energy density of a cell with Electrolyte A peaks at 116 Wh L^{-1}. Electrolyte B shows increased pH stability, resulting in improved energy density up to Zn electrode thicknesses of about 10 mm. The energy density of a cell with Electrolyte B peaks at 132 Wh L^{-1}. Electrolyte C shows a modest improvement in energy density over Electrolytes A and B, peaking at 151 Wh L^{-1}. Our simulations show that a theoretical ideal electrolyte in which only ZnO is precipitated could give rise to an energy density of 952 Wh L^{-1}, which is comparable to commercial alkaline zinc–air button cells.[1] This improvement is attributable to the lower molar volume and more favorable passivation characteristics of ZnO, as outlined in Tables 2 and 4.

Conclusions

We have developed the first continuum model to simulate the performance of zinc–air batteries (ZABs) with $ZnCl_2$–NH_4Cl electrolytes. The model is based on a quasiparticle approach to describe the dynamic behavior of buffered aqueous electrolytes. Our simulations can determine the transient and concentration-dependent behavior of the electrolyte during cell operation. The results of these simulations are in accord with existing experimental investigations from the literature and suggest topics for future research.

The thermodynamic analysis presented in this work shows that the composition of the electrolyte is complex and highly sensitive to changes in pH value, total zinc concentration, and total chloride concentration. Even small shifts in these quantities can change the state of the aqueous Zn^{2+} ion and alter the thermodynamically favored precipitate.

Cell-level simulations show that concentration and pH gradients develop in the ZAB during operation and have a significant impact on both performance and lifetime. Although $ZnCl_2$–NH_4Cl is able to buffer the pH value of the electrolyte, the practically achievable capacity of the buffer is limited by the transport of NH_3 between the gas-diffusion electrode (GDE) and the separator. For cell architectures featuring a large separator, NH_3 produced during discharge cannot be readily recovered when the cell is charged, causing the pH value in the GDE to become acidic. This effect can be mitigated by decreasing the thickness of the separator and increasing the initial pH value of the electrolyte. We propose that this effect is partially responsible for the experimentally documented gain in lifetime in the cell observed by Sumboja et al.[14] in comparison to that reported by Goh et al.[13]

We present an initial optimization of electrolyte composition and cell architecture. Electrolytes with a high initial chloride concentration will eventually converge to a lower chloride concentration near the solubility limit of $ZnCl_2{\cdot}2NH_3$ and $ZnCl_2{\cdot}4Zn(OH)_2{\cdot}H_2O$ as these solids precipitate. By altering the initial composition of the electrolyte to reflect this inevitable shift and increasing the pH value to slightly alkaline values, the system can be tuned to exclusively precipitate $Zn(OH)_2$.

The thickness of the Zn electrode should be adjusted according to the needs of the system and the composition of the electrolyte. The capacity of cells with thin Zn electrodes is limited by the passivation of zinc by the solid discharge products. Cells with thick Zn electrodes are limited by the large pH value and concentration gradients that lower the equilibrium potential of the oxygen-reduction reaction. Although tuning the cell to precipitate $Zn(OH)_2$ instead of chlorine-containing solids marginally improves the energy density of the cell, this improvement is small compared to the energy densities achievable with ZnO as the discharge product. Further research should be directed at ways to favor ZnO precipitation in the near-neutral pH regime.

Acknowledgements

*This work is supported by the European Union (EU)through the Horizon 2020 project ZAS!: Zinc Air Secondary innovative nanotech based batteries for efficient energy storage (Grant Agreement 646186). The authors wish to thank Yun Zong at the Institute of Materials Research and Engineering (IMRE) at A*STAR in Singapore for the fruitful discussion. We also acknowledge the support of the bwHPC initiative through the use of the JUSTUS HPC facility at Ulm University.*

Conflict of interest

The authors declare no conflict of interest.

Keywords: batteries · computational chemistry · electrochemistry · thermodynamics · zinc

[1] J. Stamm, A. Varzi, A. Latz, B. Horstmann, *J. Power Sources* **2017**, *360*, 136 – 149.
[2] Y. Li, H. Dai, *Chem. Soc. Rev.* **2014**, *43*, 5257 – 5275.
[3] B. Li, J. Quan, A. Loh, J. Chai, Y. Chen, C. Tan, X. Ge, T. S. A. Hor, Z. Liu, H. Zhang, Y. Zong, *Nano Lett.* **2017**, *17*, 156 – 163.
[4] P. Gu, M. B. Zheng, Q. X. Zhao, X. Xiao, H. G. Xue, H. Pang, *J. Mater. Chem. A* **2017**, *5*, 7651 – 7666.
[5] K. Wang, P. Pei, Z. Ma, H. Chen, H. Xu, D. Chen, X. Wang, *J. Mater. Chem. A* **2015**, *3*, 22648 – 22655.
[6] M. Schmid, M. Willert-Porada, *J. Power Sources* **2017**, *351*, 115 – 122.
[7] D. Kundu, B. D. Adams, V. Duffort, S. H. Vajargah, L. F. Nazar, *Nat. Energy* **2016**, *1*, 16119.
[8] J.-I. Jung, M. Risch, S. Park, M. G. Kim, G. Nam, H.-Y. Jeong, Y. Shao-Horn, J. Cho, *Energy Environ. Sci.* **2016**, *9*, 176 – 183.
[9] K. E. K. Sun, T. K. A. Hoang, T. N. L. Doan, Y. Yu, X. Zhu, Y. Tian, P. Chen, *ACS Appl. Mater. Interfaces* **2017**, *9*, 9681 – 9687.
[10] J. Fu, Z. P. Cano, M. G. Park, A. Yu, M. Fowler, Z. Chen, *Adv. Mater.* **2017**, *29*, 1604685.
[11] T. Arlt, D. Schröder, U. Krewer, I. Manke, *Phys. Chem. Chem. Phys.* **2014**, *16*, 22273 – 22280.
[12] J. Jindra, J. Mrha, M. Musilová, *J. Appl. Electrochem.* **1973**, *3*, 297 – 301.
[13] F. W. T. Goh, Z. Liu, T. S. A. Hor, J. Zhang, X. Ge, Y. Zong, A. Yu, W. Khoo, *J. Electrochem. Soc.* **2014**, *161*, A2080 – A2086.
[14] A. Sumboja, X. Ge, G. Zheng, F. W. T. Goh, T. S. A. Hor, Y. Zong, Z. Liu, *J. Power Sources* **2016**, *332*, 330 – 336.
[15] R. Winand, *Modern Electroplating*, Wiley, Hoboken, New Jersey, **2011**.
[16] H. Pan, Y. Shao, P. Yan, Y. Cheng, K. S. Han, Z. Nie, C. Wang, J. Yang, X. Li, P. Bhattacharya, K. T. Mueller, J. Liu, *Nat. Energy* **2016**, *1*, 16039.
[17] D. U. Lee, P. Xu, Z. P. Cano, A. G. Kashkooli, M. G. Park, Z. Chen, *J. Mater. Chem. A* **2016**, *4*, 7107 – 7134.
[18] B. Lee, H. R. Seo, H. R. Lee, C. S. Yoon, J. H. Kim, K. Y. Chung, B. W. Cho, S. H. Oh, *ChemSusChem* **2016**, *9*, 2948 – 25956.

[19] X. G. Zhang, *Corrosion and Electrochemistry of Zinc*, Plenum Press, New York, NY, **1996**.
[20] J. L. Limpo, A. Luis, M. C. Cristina, *Hydrometallurgy* **1995**, *38*, 235 – 243.
[21] J. L. Limpo, A. Luis, *Hydrometallurgy* **1993**, *32*, 247 – 260.
[22] M. Winter, R. J. Brodd, *Chem. Rev.* **2004**, *104*, 4245 – 4269.
[23] A. M. Bredland, M. N. Hull, *J. Electrochem. Soc.* **1976**, *123*, 311 – 315.
[24] H. F. McMurdie, D. N. Craig, G. W. Vinal, *J. Electrochem. Soc.* **1946**, *90*, 509 – 528.
[25] R. Friess, *J. Am. Chem. Soc.* **1930**, *52*, 3083 – 3087.
[26] S. Zhao, H. An, S. Chen, *J. Power Sources* **1998**, *76*, 218 – 220.
[27] A. R. Mainar, L. C. Colmenares, O. Leonet, F. Alcaide, J. J. Iruin, S. Weinberger, V. Hacker, E. Iruin, I. Urdanpilleta, J. A. Blazquez, *Electrochim. Acta* **2016**, *217*, 80 – 91.
[28] R. Smith, A. Martell, *Critical Stability Constants Volume 4: Inorganic Complexes*, Plenum Press, New York, NY, **1976**.
[29] E. Deiss, F. Holzer, O. Haas, *Electrochim. Acta* **2002**, *47*, 3995 – 4010.
[30] D. Schröder, U. Krewer, *Electrochim. Acta* **2014**, *117*, 541 – 553.
[31] W. G. Sunu, D. N. Bennion, *J. Electrochem. Soc.* **1980**, *127*, 2007 – 2016.
[32] Z. Mao, R. E. White, *J. Electrochem. Soc.* **1992**, *139*, 1105 – 1114.
[33] J. Vazquez-Arenas, F. Sosa-Rodriguez, I. Lazaro, R. Cruz, *Electrochim. Acta* **2012**, *79*, 109 – 116.
[34] T. P. Dirkse, *J. Electrochem. Soc.* **1986**, *133*, 1656 – 1657.
[35] N. C. Cahoon, *J. Electrochem. Soc.* **1947**, *92*, 159 – 172.
[36] J. Larcin, W. C. Maskell, F. L. Tye, *Electrochim. Acta* **1997**, *42*, 2649 – 2658.
[37] B. Horstmann, T. Danner, W. G. Bessler, *Energy Environ. Sci.* **2013**, *6*, 1299.
[38] J. P. Neidhardt, D. N. Fronczek, T. Jahnke, T. Danner, B. Horstmann, W. G. Bessler, *J. Electrochem. Soc.* **2012**, *159*, A1528 – A1542.
[39] A. Latz, J. Zausch, *Electrochim. Acta* **2013**, *110*, 358 – 362.
[40] M. Z. Bazant, *Acc. Chem. Res.* **2013**, *46*, 1144 – 1160.
[41] D. Eberle, B. Horstmann, *Electrochim. Acta* **2014**, *137*, 714 – 720.
[42] F. Single, B. Horstmann, A. Latz, *Phys. Chem. Chem. Phys.* **2016**, *18*, 17810 – 17814.
[43] T. Danner, S. Eswara, V. P. Schulz, A. Latz, *J. Power Sources* **2016**, *324*, 646 – 656.
[44] M. D. Radin, C. W. Monroe, D. J. Siegel, *Chem. Mater.* **2015**, *27*, 839 – 847.
[45] T. Danner, B. Horstmann, D. Wittmaier, N. Wagner, W. G. Bessler, *J. Power Sources* **2014**, *264*, 320 – 332.
[46] D. G. Miller, A. W. Ting, J. A. Rard, *J. Electrochem. Soc.* **1988**, *135*, 896 – 903.
[47] J. A. Rard, D. G. Miller, *J. Solution Chem.* **1990**, *19*, 129 – 148.
[48] J. Newman, K. E. Thmoas-Alyea, *Electrochemical Systems*, Wiley, Hoboken, NJ, **2004**.
[49] M. Qaiser Fatmi, T. S. Hofer, B. M. Rode, *Phys. Chem. Chem. Phys.* **2010**, *12*, 9713 – 9718.
[50] K. Sasaki, T. Takahashi, *Electrochim. Acta* **1959**, *1*, 261 – 271.
[51] P. Atkins, J. De Paula, *Atkins' Physical Chemistry*, W. H. Freeman And Company, New York **2006**.
[52] E. L. Shock, H. C. Helgeson, *Geochim. Cosmochim. Acta* **1988**, *52*, 2009 – 2036.
[53] E. L. Shock, H. C. Helgeson, D. A. Sverjensky, *Geochim. Cosmochim. Acta* **1989**, *53*, 2157 – 2183.
[54] E. L. Shock, D. C. Sassani, M. Willis, D. A. Sverjensky, *Geochim. Cosmochim. Acta* **1997**, *61*, 907 – 950.
[55] D. A. Sverjensky, E. L. Shock, H. C. Helgeson, *Geochim. Cosmochim. Acta* **1997**, *61*, 1359 – 1412.
[56] A. Roux, G. M. Musbally, G. Perron, J. E. Desnoyers, *Can. J. Chem.* **1978**, *56*, 24 – 28.
[57] M. J. W. Frank, J. A. M. Kuipers, W. P. M. Van Swaaij, *J. Chem. Eng. Data* **1996**, *41*, 297 – 302.
[58] Z. Huajun, G. Zhenghai, Z. Jinhuan, *Hydrometallurgy* **2007**, *89*, 369 – 373.
[59] I. Roche, K. Scott, *J. Appl. Electrochem.* **2009**, *39*, 197 – 204.
[60] T. Takashima, K. Hashimoto, R. Nakamura, *J. Am. Chem. Soc.* **2012**, *134*, 1519 – 1527.
[61] F. Single, B. Horstmann, A. Latz, *J. Electrochem. Soc.* **2017**, *164*, E3132 – E3145.
[62] M. Huynh, D. K. Bediako, D. G. Nocera, *J. Am. Chem. Soc.* **2014**, *136*, 6002 – 6010.
[63] T. Takashima, K. Hashimoto, R. Nakamura, *J. Am. Chem. Soc.* **2012**, *134*, 18153 – 18156.
[64] R. Pokhrel, M. K. Goetz, S. E. Shaner, X. Wu, S. S. Stahl, *J. Am. Chem. Soc.* **2015**, *137*, 8384 – 8387.
[65] Q. C. Horn, Y. Shao-Horn, *J. Electrochem. Soc.* **2003**, *150*, A652 – A658.

Manuscript received: August 7, 2017
Accepted manuscript online: September 12, 2017
Version of record online: November 16, 2017

